NANO LETTERS

Letter

pubs.acs.org/NanoLett

Rational Design of "Heat Seeking" Drug Loaded Polypeptide Nanoparticles That Thermally Target Solid Tumors

Jonathan R. McDaniel,[†] Sarah R. MacEwan,[†] Xinghai Li,[†] D. Christopher Radford,[†] Chelsea D. Landon,[‡] Mark Dewhirst,[‡] and Ashutosh Chilkoti*[,†]

[†]Department of Biomedical Engineering, Duke University, Durham, North Carolina 27708-0281, United States

[‡]Department of Radiation Oncology, Duke University, Durham, North Carolina 27708-0281, United States

Supporting Information

ABSTRACT: This paper demonstrates the first example of targeting a solid tumor that is externally heated to 42 °C by "heat seeking" drug-loaded polypeptide nanoparticles. These nanoparticles consist of a thermally responsive elastin-like polypeptide (ELP) conjugated to multiple copies of a hydrophobic cancer drug. To rationally design drug-loaded nanoparticles that exhibit thermal responsiveness in the narrow temperature range between 37 and 42 °C, an analytical model was developed that relates ELP composition and chain length to the nanoparticle phase transition temperature. Suitable candidates were designed based on the predictions of the model and tested in vivo by intravital confocal fluorescence microscopy of solid tumors, which revealed that the nanoparticles aggregate in the vasculature of tumors heated to 42 °C and that the aggregation is reversible as the temperature reverts to 37 °C. Biodistribution studies showed that the most effective strategy to target the nanoparticles to tumors is to thermally cycle the tumors between 37 and 42 °C. These nanoparticles set the stage for the targeted delivery of a range of cancer chemotherapeutics by externally applied mild hyperthermia of solid tumors.

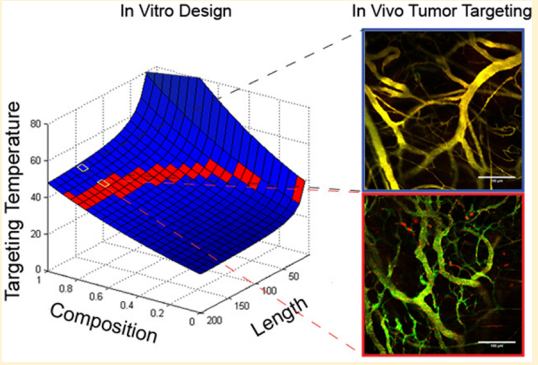

KEYWORDS: *Elastin-like polypeptides, thermal targeting, drug delivery, hyperthermia, thermosensitive, nanoparticles*

Small molecule chemotherapeutics have limited clinical effectiveness, as their poor pharmacokinetics lead to rapid clearance from circulation and their exposure to off-target tissues results in dose-limiting toxicity. The use of macromolecular carriers to ferry drugs to solid tumors improves their therapeutic efficacy by increasing plasma retention time, reducing uptake by healthy tissues, and enhancing tumor accumulation by passively exploiting the enhanced permeability and retention (EPR) effect that is exhibited by many solid tumors.[1] Furthermore, active targeting strategies such as attaching ligands,[2] aptamers,[3] and antibodies[2,4] to macromolecular carriers can further increase tumor drug levels by specifically targeting receptors that are overexpressed by cells in the tumor. However, these strategies are limited by two factors: (1) the binding site barrier, in which the high affinity between the carrier and the targeted molecule prevents diffusion beyond the tumor periphery[5] and (2) the heterogeneity of tumor tissue, as the level of receptor overexpression varies significantly across different tumors,[6,7] between patients with the same type of cancer,[8] and spatially within each tumor.[8,9] Tumor targeting strategies that can circumvent these limitations are hence of great interest.

Herein, we demonstrate a proof-of-principle of an alternative targeting strategy in which "heat seeking" drug-loaded polypeptide nanoparticles thermally target a tumor that is externally heated to 42 °C, a temperature that we chose because it is compatible with the clinical use of mild-hyperthermia of solid tumors.[10,11] This work builds upon—but departs significantly from—our previous work on drug-loaded polypeptide nanoparticles. In our initial implementation of drug-loaded nanoparticles,[10,12] we designed recombinant chimeric polypeptide (CP) nanoparticles that consist of a thermally responsive elastin-like polypeptide fused to a cysteine-rich peptide tail to which small molecule therapeutics can be attached covalently. We previously showed that the attachment of doxorubicin to a CP triggers self-assembly of the peptides into nanoparticles and that these nanoparticles are effective in treating solid tumors upon i.v. injection.[12] We subsequently showed that CPs also self-assemble upon attachment of diverse hydrophobic small molecules, making them a versatile system for the delivery of small molecule drugs.[10] However, these first generation CP−drug nanoparticles were not designed to display thermal sensitivity within the clinically relevant temperature regime of 40−45 °C that defines the approved temperatures for mild hyperthermia of solid tumors,[13,14] as they displayed a nanoparticle-to-aggregate transition temperature (T_t) well above 50 °C.

Received: March 12, 2014
Revised: April 14, 2014
Published: April 16, 2014

To design a "heat seeking" CP−drug nanoparticle that can exhibit preferential accumulation in tumors heated to 42 °C is not trivial because the molecular parameters that govern the phase transition behavior of drug-loaded nanoparticles have never been quantified. To this end, we first developed an analytical model that quantitatively predicts the nanoparticle T_t in terms of three design variables—CP sequence, chain length, and solution concentration. Next, we used this model to rationally design doxorubicin (Dox) containing CP nanoparticles that display a T_t between 39 °C (slightly above physiological temperature) and 42 °C. This is representative of a temperature that can be achieved in the majority of tumors, while avoiding pain and/or normal tissue damage.[14] The thermal reversibility and in vivo thermal transition of the nanoparticles were validated by intravital confocal fluorescence microscopy using a dorsal skin fold tumor window chamber model. The in vivo distribution of the drug demonstrated that the application of mild hyperthermia induces the site-specific accumulation of thermally responsive CP nanoparticles within tumors and that thermal cycling of tumors results in a 2.6-fold greater accumulation of CP−Dox nanoparticles in the tumor compared to tumors that are not heated. This heat-mediated preferential delivery indicates that this approach can be used to target drugs to tumors through the application of mild hyperthermia.

Drug-loaded chimeric polypeptide nanoparticles are composed of thermally responsive elastin-like polypeptides (ELPs) with short cysteine-rich peptide tails that self-assemble into micelles upon conjugation of hydrophobic drugs to the cysteine residues. The ELP segment consists of a pentameric repeat, VPGXG, where the hydrophobicity of the guest residue "X" and the length of the polypeptide modulate the T_t of the ELP.[15,16] Similar to their parent ELPs, CP nanoparticles also exhibit a thermally triggered phase transition from soluble nanoparticles to an aggregated phase above their T_t. Importantly, the T_t of these nanoparticles is nearly independent of the CP concentration and the structure of the conjugated molecule, as long as the molecule displays an octanol−water distribution coefficient (LogD) > 1.5.[10] The stability of the T_t in response to dilution and its insensitivity to the structure of the conjugated molecule suggests that this system is well-suited for the thermally targeted delivery of structurally diverse hydrophobic drugs via attachment triggered self-assembly in vivo.

Because CP−Dox nanoparticles in our previous work displayed an in vivo T_t of ∼50 °C,[10,12] we had to design new CP nanoparticles that would be responsive within the desired physiological range of 39−42 °C. To generate a model that can predict a priori the T_t of CP nanoparticles, we synthesized 24 unique CPs with different ELP segments and an invariant drug attachment $(Cys\text{-}Gly\text{-}Gly)_8$ peptide tail that was fused to their C-terminus (Figures S1 and S2 of the Supporting Information (SI)). The drug attachment segment has eight cysteines that provide unique thiols for site-specific conjugation separated by digylcine spacers to reduce steric hindrance between the conjugated molecules. To generate this model, we expressed and purified all 24 constructs (Figure S3 of the SI) and conjugated *n*-benzyl maleimide to the cysteine residues in each CP. We chose *n*-benzyl maleimide as the model hydrophobe because it is inexpensive, reacts rapidly with the CP, and displays sufficient hydrophobicity to drive assembly of CP nanoparticles. As we have previously shown that the T_t of CP nanoparticles is not dependent upon the molecular structure of the attached molecule (as long as its LogD > 1.5),[10] we hypothesized that a single molecule should accurately predict the T_t of CP nanoparticles for a wide variety of hydrophobic therapeutics.

The thermal properties of the 24 unique CP nanoparticles were then measured as a function of CP concentration in phosphate-buffered saline (PBS) (Figure S4 of the SI) and fit by multivariate analysis to arrive at eq 1:

$$T_t = 20.0e^{0.8\times f\text{-Alanine}} + \frac{17.1e^{1.2\times f\text{-Alanine}}}{\text{Length}}[\ln 6.4\times 10^6 - 0.4\times f\text{-Alanine} - \ln(\text{Conc})] \quad (1)$$

where T_t represents the transition temperature, Length is the number of pentapeptide repeats, Conc is the solution concentration of the ELP in μM, and *f*-Alanine represents the ratio of alanines to the total number of guest residue positions (with the remaining positions occupied by valine).[15] This model describes 99% of the variability in the experimental data (Figure 1A; r^2 = 0.994; n = 120). Figure 1B illustrates the dependence of the T_t, which varies from 21.2 to 64.8 °C, on composition and molecular weight (for a CP unimer concentration of 25 μM). This model enabled the selection of discrete molecular weight and composition pairs that display

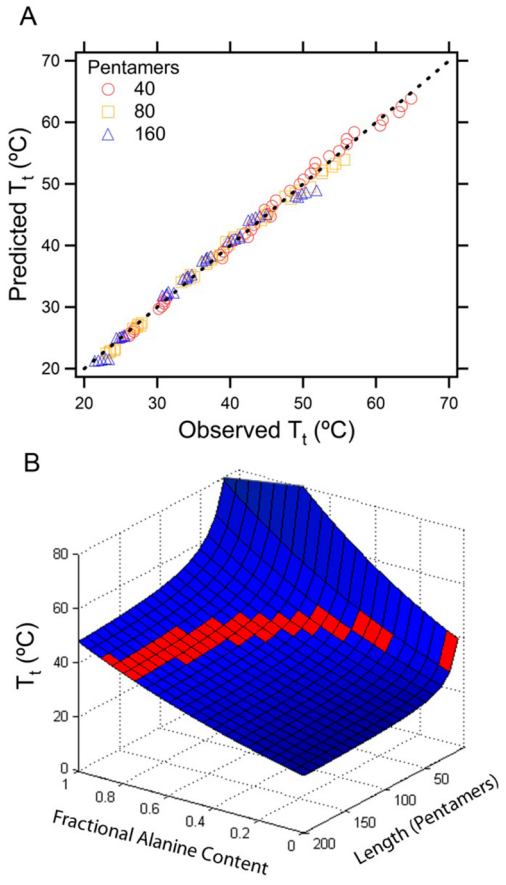

Figure 1. (A) Predicted versus observed T_t for a global fit of CP nanoparticles in PBS (r^2 = 0.994; n = 120). The CP nanoparticles were generated through the conjugation of *n*-benzyl maleimide to the C-terminal cysteine residues. (B) The model was used to predict the composition and length of a family of thermally responsive (39−42 °C) CP nanoparticles (shown in red) at a concentration typical for drug delivery using CPs (25 μM) in PBS.

dx.doi.org/10.1021/nl5009376 | *Nano Lett.* 2014, 14, 2890−2895

a sharp phase transition in response to mild hyperthermia in PBS (Figure 1B; red squares). To examine the hypothesis that this model accurately predicts the T_t of CPs attached to compounds other than *n*-benzyl maleimide, three CPs that exhibited T_t's between 39 and 42 °C were expressed, purified, and conjugated to *n*-benzyl maleimide, *n*-pyrenyl malemide, and doxorubicin. We found that their experimentally measured T_t was within 1 °C of their predicted T_t despite significant differences in the structure and molecular weight of the molecules (Table S1 of the SI), showing that this model provides a good estimate of the T_t for a variety of CP−drug nanoparticles.

We next examined the thermal behavior of the CP nanoparticles in a physiologically relevant medium because ions and proteins in serum lower the T_t from the values measured in PBS.[17] To mimic the vascular environment, we measured the thermal behavior of the CP nanoparticles in 90% fetal bovine serum (FBS) at 50 μM, which falls within the concentration regime relevant to systemic drug delivery (Figure 2A). The thermal transition profiles of nanoparticles created by conjugation to *n*-benzyl maleimide and those created by the attachment of *n*-pyrenyl maleimide and doxorubicin were indistinguishable (less than a 1 °C difference in their nanoparticle−aggregate T_t) in 90% FBS (Table S2 of the SI), which suggests that the curves in Figure 2A can be used to predict the T_t for a variety of CP nanoparticle conjugates in vivo. It can also be seen that the three CP−drug nanoparticles selected for doxorubicin attachment (indicated by arrows in Figure 2) represent potential compositions at each length (40, 80, and 160 pentamers) that display a thermally triggered nanoparticle-to-aggregate phase transition under conditions of mild hyperthermia.

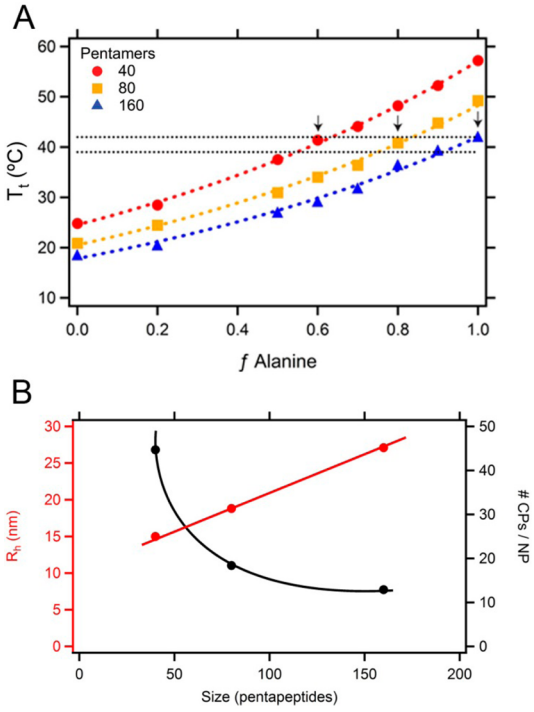

Figure 2. (A) Observed (markers) T_t for CP nanoparticles (conjugated to *n*-benzyl maleimide) in 90% FBS. Dashed lines represent the best exponential fit. Black dashed lines demarcate the targeted range of hyperthermia (39−42 °C). Indicated constructs (arrows) represent those selected for additional in vivo biodistribution and pharmacokinetic studies. (B) Light scattering analysis of three CP−Dox nanoparticle constructs. The points in red represent the hydrodynamic radius (R_h), and the points in black represent the average number of CPs per nanoparticle (#CPs/NP) as calculated by dividing the absolute molecular weight of the micelle by the molecular weight of the CP. The lines are simply a guide to the eye.

The model presented in Figure 1 (T_t in PBS) indicates that there are many binary combinations of chain length and sequence that yield unique CPs exhibiting a nanoparticle−aggregate phase transition within the narrow temperature window of 39−42 °C. To narrow the field of candidates, we selected CPs with three different molecular weights (15 kDa or 40 pentapeptides; 30 kDa or 80 pentapeptides; and 60 kDa or 160 pentapeptides) for more detailed characterization for two reasons. First, these sizes span the molecular weight range of the CPs used to construct the mathematical model, so that testing their thermal phase behavior would help provide further validation of the model. Second, CPs in this size range are above (60 kDa) and below (30 and 15 kDa) the estimated renal filtration cutoff, thus allowing us to study the impact of molecular weight on the in vivo clearance of these nanoparticles.[18,19]

To examine how the molecular weight of the CP influences the physicochemical properties of the nanoparticles, each of these constructs was separately conjugated to doxorubicin via an acid labile heterobifunctional linker to drive self-assembly into nanoparticles and enable intracellular release of the drug once exposed to the low pH of the late endosome (Figure S5 of the SI).[12] Upon conjugation, the CPs spontaneously assembled into micelles with a hydrodynamic size that linearly correlated with chain length (Figure 2B). The hydrodynamic radius (R_h) varied from 15 nm for the CP−Dox micelles composed of the 40 pentamer CP to 27 nm for CP−Dox micelles composed of the 160 pentamer construct. Static light scattering analysis indicated that the average number of CP molecules per micelle was inversely proportional to the CP chain length (Figure 2B). Micelles composed of 160 VPGXG pentamer units consisted of 13 CP molecules per nanoparticle. In contrast, 80 pentamer units contained 18 molecules per nanoparticle, and the 40 pentamer units contained 45 molecules per nanoparticle.

After verifying that doxorubicin conjugation triggered self-assembly of the CP into micelles, we next examined the effect of CP chain length on in vitro cytotoxicity. C26 cells isolated from a murine colon adenocarcinoma were exposed to CP−Dox nanoparticles over a wide range of concentrations (0.001−60 μM Dox equivalents) for a period of 72 h. Following this incubation period, a 3-(4,5-dimethylthiazol-2-yl)-5-(3-carboxymethoxyphenyl)-2-(4-sulfophenyl)-2*H*-tetrazolium (MTS) assay was performed to measure the metabolic viability of the cells as measured by the concentration of drug necessary to inhibit cellular proliferation by 50% (IC_{50}). We observed that CP chain length did not significantly alter the measured IC_{50} (free Dox: 0.2 ± 0.1 μM; 40 pentamer CP: 2.6 ± 0.8 μM; 80 pentamer CP: 1.7 ± 0.5 μM; and 160 pentamer CP: 1.5 ± 0.2 μM; Figure S6 of the SI). However, similar to other systems that rely on chemical conjugation of drug, conjugation to the CPs resulted in an approximately 11-fold reduction in *in vitro* cytotoxicity compared to free doxorubicin.[12,20,21]

To determine the pharmacokinetic parameters of the CP−Dox nanoparticles, the plasma doxorubicin concentration was longitudinally tracked over a period of 48 h following systemic administration to mice via tail vein injection (Figure 3A) and fit to a two-compartment model. Table 1 shows that chain length

dx.doi.org/10.1021/nl5009376 | *Nano Lett.* 2014, 14, 2890−2895

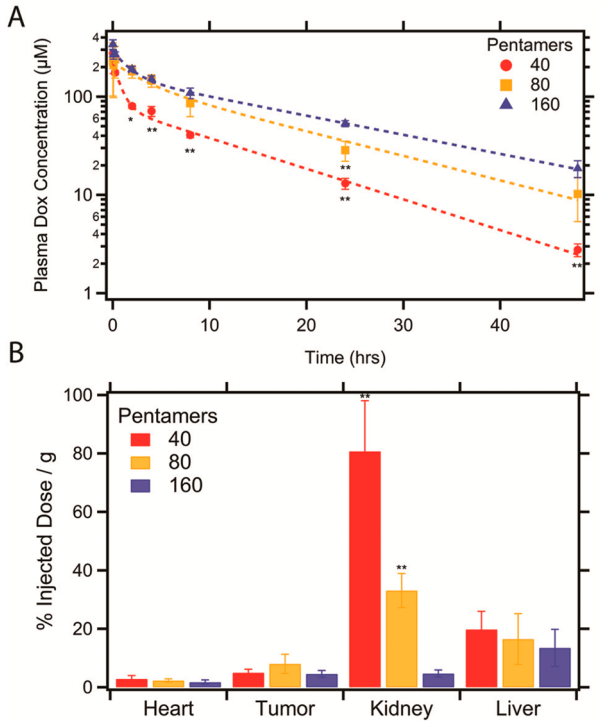

Figure 3. (A) Plasma concentration of doxorubicin-loaded CP nanoparticles following systemic administration into mice. The data points represent the mean ± SD (n = 3), and the dashed lines represent the curves of best fit to the two-compartment model by SAAM II. (B) Distribution of doxorubicin within select organs 24 h post administration. Data represent the mean ± SD with n = 3 mice. The significance (one-way ANOVA, Tukey posthoc) was calculated for the 40 and 80 pentamer constructs for all time points. *p < 0.05 and **p < 0.005 against the 160 pentapeptide construct.

plays a significant role in the pharmacokinetics of CP−Dox micelles, with the 160 pentamer construct exhibiting an elimination half-life of 15.5 h, followed by the 80 pentamer construct at 12.1 h, and the 40 pentamer construct at 9.6 h (see Table S3 of the SI for the complete list of parameters). The plasma concentration profile is also an important determinant for the efficacy of many macromolecular drug carriers. Similar to the half-life, the relative AUC (area under the time−concentration curve) was the greatest for the longest chain length (160 pentamers) and decreased to 72% of the 160 pentamer length for the 80 pentamer CP and 32% for the 40 pentamer CP.

Following pharmacokinetic analysis, we evaluated the biodistribution of the three conjugates with the goal of selecting the conjugate with the lowest level of accumulation within the heart for further in vivo studies. Reduction of the doxorubicin levels in the heart is particularly critical, as cardiomyopathy is the primary dose-limiting factor for doxorubicin treatment in the clinic. Mice were administered CP−Dox via tail vein injection, and the tumor, which was inoculated on the right flank of the mouse, was immediately heated to 42 °C via water bath for 1 h. The mice were sacrificed 24 h following administration, and the doxorubicin concentration within tissues was quantified by a fluorescence assay.

The doxorubicin level was examined in each of seven primary tissues 24 h following i.v. administration (Figure S7 of the SI). In general, accumulation correlated with chain length, with higher molecular weight constructs showing a decrease in accumulation in certain organs. This effect was most notable in the kidneys, which exhibited a marked decrease in accumulation with increasing CP molecular weight from ∼80% injected dose (%ID/g) for the 40 pentamer construct to 5% ID/g for the 160 pentamer construct. Similarly, compared to the 40 pentamer construct, the 160 pentamer conjugate also demonstrated a 33% reduction in liver accumulation and a 40% reduction in heart accumulation (Figure 3B), supporting the results observed in the two-compartmental pharmacokinetic model. Future studies would benefit from performing bone marrow analysis, as this also represents a primary target of doxorubicin toxicity.[22]

The finding that micelles assembled from chains of varying molecular weight exhibit an altered pharmacokinetic and biodistribution profile suggests that the molecular weight of the individual chains comprising the higher order self-assembled structure is a critical design parameter. This observation is likely a result of continual renal filtration of the CP molecules, whose molecular weight is below the estimated renal filtration cutoff of 50 kDa for both the 40 (15 kDa) and 80 (30 kDa) pentamer constructs, as noncovalently assembled systems like micelles exist in dynamic equilibrium with their single chain constituents. In fact, this phenomenon has been observed in a variety of systems including diblock micelles[23] and multisubunit enzymes.[24] Nevertheless, we note that the size of the micelles also scales with their molecular weight, so that unambiguous discrimination between the effects of the micelle size and the molecular weight of the constituent polymer chains on the pharmacokinetics and biodistribution would require control experiments with cross-linked micelles composed of nearly identical components.

These data, in combination with the pharmacokinetic profile, indicate that micelles consisting of higher molecular weight CP retain doxorubicin in the plasma for a longer period of time (longer half-life), thereby increasing the overall exposure of the tumor vasculature to the drug (higher AUC). Furthermore, they also exhibit a lower concentration of drug within critical healthy tissues, thus potentially reducing systemic toxicity. In particular, the high overall drug accumulation in the kidneys for the shorter length CPs suggest that the 160 pentamer construct would provide both an enhanced antitumor effect over shorter chain lengths and a significant reduction in off-target toxicities. Hence, we selected the 160 pentamer chain length for use in all subsequent in vivo studies.

We first confirmed that the micelles reversibly phase separate in vivo within the thermal range of 39−42 °C. To accomplish this, we utilized a dorsal skin fold tumor window chamber

Table 1. Half-Life and AUC of CP−Dox Micelles Composed of CPs with Varying Sizes[a]

parameter		40 pentamers	80 pentamers	160 pentamers
elimination half-life	β $t_{1/2}$ (h)	9.6 (0.4)	12.1 (1.0)	15.5 (0.9)
area under the curve	AUC (μM·h)	1202.9 (42.8)	2690.5 (119.6)	3734.6 (112.3)

[a]Data represent the mean (SD) of the best fit parameters determined by SAAM II.

dx.doi.org/10.1021/nl5009376 | Nano Lett. 2014, 14, 2890−2895

model, which allows visualization of the tumor vasculature in real time under a confocal microscope. We examined three CP micelles: (1) a hydrophilic control with an ELP chain length of 160 pentamers and a guest residue composition of X = Ala_1Gly_1: this micelle aggregates at 50 °C in physiological media and hence should not display thermal sensitivity within the range of 39−42 °C; (2) a thermally responsive formulation of 160 pentamers and a guest residue ratio of X = Ala_9Val_1 that aggregates at 39 °C in physiological media; and (3) a thermally responsive formulation of 160 pentamers and a guest residue of Ala that displays a phase transition at 42 °C. Each of the CPs was labeled at their N-terminus with a rhodamine derivative, which provides red fluorescence but does not perturb self-assembly or the micelle-to-aggregate T_t. The CPs were self-assembled into spherical micelles through the attachment of *n*-pyrenyl malemide to the unique cysteine residues at the C-terminus. Pyrenyl malemide was selected over doxorubicin for these experiments because rhodamine fluorescence was significantly diminished in the presence of doxorubicin.

A large molecular weight (2 MDa) dextran conjugated to fluorescein was coinjected with the CP micelles to provide a distinct green vascular mask. The color balance was then adjusted to provide a yellow overlay in the presence of both soluble green dextran and soluble red CP micelles. As the control CP has a T_t > 42 °C, it is homogeneously distributed throughout the vasculature at both 37 and 42 °C (Figure 4A, B). In contrast, the thermally responsive CP micelle formulation, which phase separates at 39 °C, is soluble at 37 °C, as observed by the homogeneous yellow overlay. However, as the tumor is heated to 42 °C, the CP micelles exhibited a rapid and robust phase separation into micrometer-sized hydrophobic particles seen throughout the vasculature (Figure 4C, D). We also observed that the degree of phase separation could be controlled by specifying the T_t. While heating to 42 °C was sufficient to induce a response in the CP nanoparticles with a T_t = 42 °C (Figure S8A of the SI, image taken after 30 min of heating), it was not nearly as robust a response as seen for the CP nanoparticles that display a T_t of 39 °C (Figure S8B of the SI; image taken after 10 min of heating). Hence, lowering the T_t results in a greater thermodynamic driving force for phase separation measured as the difference between the T_t and the temperature in the window chamber. For this reason, the more thermally responsive construct (T_t = 39 °C) was selected for biodistribution analysis.

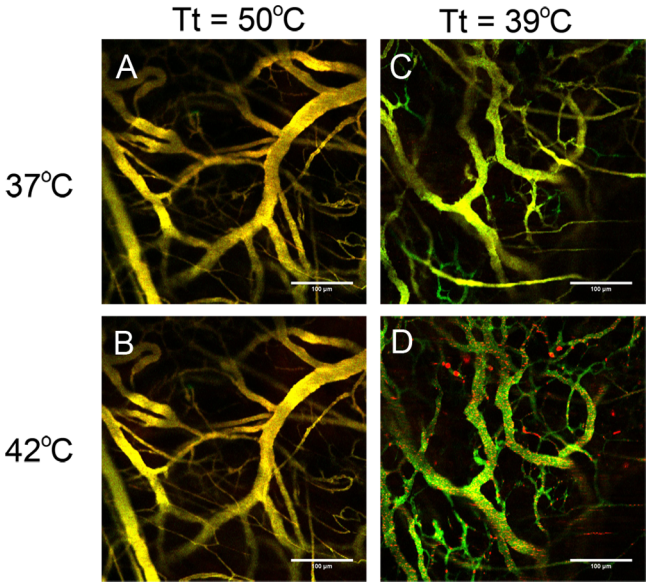

Figure 4. In vivo visualization of the phase transition in response to heat. A control CP micelle formation with a T_t of 50 °C remained soluble when heated to (A) 37 °C and (B) 42 °C for 10 min each. A thermally responsive micelle formulation that transitions at 39 °C remains soluble at (C) 37 °C but phase separates at (D) 42 °C after 10 min. Scale bars represent 100 μm. Scale bars represent 100 μm. Red represents ELP; green represents tumor vasculature.

Figure 4 does not do clear justice to the stunning degree of aggregation we observed for the thermally responsive micelle at 42 °C. Videos S1 and S2 of the SI, accrued over low 10× magnification, show a high degree of phase separation in the vasculature within the first 30 min at 42 °C when compared to the same construct at 37 °C (Video S3 of the SI). The aggregated micelles largely fill the tumor microvasculature and in one instance occlude a fairly large vein.

With a clear phase separation occurring selectively between the vasculature heated to 37 °C and that heated to 42 °C, we next examined whether the phase transition was reversible under physiological conditions. Figure S9 of the SI shows images of the green (fluorescein−dextran) and red (CP−rhodamine) channels as the temperature is slowly ramped from 37 to 42 °C and then decreased to 37 °C. At 37 °C, the CP micelles are homogeneously distributed throughout the vasculature. As the temperature approaches 42 °C, the micelles coalesce into discrete particles (visualized by their punctate red fluorescence) that fully dissipate upon cooling to 37 °C.

Finally, we examined whether triggering the phase transition increased drug accumulation within the tumor. To test this hypothesis, we administered the control (T_t = 50 °C) and thermally responsive (T_t = 39 °C) CP−Dox micelles to balb/c mice bearing a murine C26 colon carcinoma in their hind leg. Each treatment was then subdivided into three experimental cohorts: mice receiving: (1) no thermal therapy; (2) 1 h of hyperthermia applied by submerging the hind leg of the mouse in a water bath heated to 42 °C; and (3) 1 h of hyperthermia divided into six intervals of 10 min of heat followed by 10 min without heat (Figure 5). The mice were sacrificed 2 h following administration of the drug, and the Dox concentration in the tumor was measured via a fluorescence assay. Surprisingly, 1 h of hyperthermia increased the accumulation of Dox within the

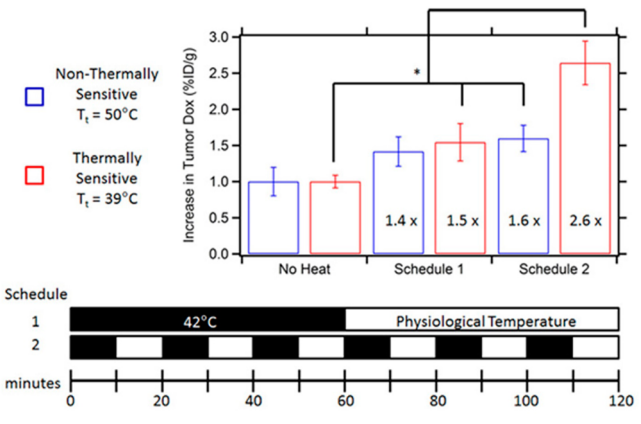

Figure 5. Tumor biodistribution of a thermally responsive and a control CP−Dox nanoparticle formulation following two heating schedules. Mice were sacrificed 120 min following drug administration. *p < 0.05.

dx.doi.org/10.1021/nl5009376 | *Nano Lett.* 2014, 14, 2890−2895

tumor by 50% for both CP−Dox constructs, implying that the effects of hyperthermia—and not the phase transition—dominated the biodistribution of the CP carrier under these conditions. However, when the same 1 h of hyperthermia was divided into six separate heating and cooling cycles, the control CP showed the same ∼50% increase in accumulation, while the thermally responsive CP exhibited a 160% increase ($p < 0.001$).

We hypothesize that, because the physiological temperature is below the T_t in systemic circulation, the CP circulates as a soluble nanoparticle; upon reaching a heated tumor in which the temperature is above the T_t, the CP undergoes its phase transition and forms micrometer-sized aggregates that adhere to the tumor vasculature. Upon cessation of hyperthermia, the rapid resolubilization of the CP aggregates creates a steep transvascular concentration gradient that drives CP extravasation into the tumor by diffusion.[25] This hypothesis suggests that the accumulation of drug positively correlates with the number of heating and cooling cycles, and thus it may be possible to further augment the efficacy of this strategy by simply increasing the number of cycles. This is currently under investigation.

This work demonstrates that the micelle-to-aggregate T_t of CP nanoparticles can be predicted by their sequence, chain length, and concentration. We directly confirmed by intravital fluorescence microscopy that the phase separation occurs in the narrow temperature range of 39−42 °C in vivo in the heated tumor vasculature and that it is reversible. Thermally cycling the tumors following injection of the thermally responsive CP−Dox nanoparticles resulted in significantly enhanced drug accumulation over nonthermally responsive nanoparticles. This increase is consistent with the creation of a steep transvascular CP−Dox concentration gradient upon cooling that pumps the soluble conjugate across the vascular and interstitial fluid pressure barrier by diffusion. These results suggest that thermally cycling tumors will provide a significant boost in efficacy for thermally responsive CP−drug nanoparticles.

■ ASSOCIATED CONTENT

Supporting Information

Materials and methods. Oligomer sequences, SDS-PAGE gels, thermal turbidimetry plots, IC_{50} profiles, chemical synthesis schematic, detailed pharmacokinetic parameters, biodistribution data, intravital microscopy images, and videos. This material is available free of charge via the Internet at http://pubs.acs.org.

■ AUTHOR INFORMATION

Corresponding Author

*E-mail: chilkoti@duke.edu.

Present Addresses

J.R.M.: Department of Chemical Engineering, Institute for Molecular and Cellular Biology, University of Texas at Austin, Austin, TX 78712−1062.

D.C.R.: Department of Bioengineering, University of Utah, Salt Lake City, UT 84112.

Notes

The authors declare no competing financial interest.

■ ACKNOWLEDGMENTS

We would like to thank Eric Mastria for assistance with mouse studies. This work was partially supported by a grant from the National Institutes of Health (R01 EB000188) to A.C. and by the NSF through the Research Triangle MRSEC (NSF-DMR-11-21107).

■ REFERENCES

(1) Maeda, H. *J. Controlled Release* **2012**, *164*, 138.
(2) Torchilin, V. P. *Cell. Mol. Life Sci.* **2004**, *61*, 2549.
(3) Farokhzad, O. C.; Jon, S. Y.; Khademhosseini, A.; Tran, T. N. T.; LaVan, D. A.; Langer, R. *Cancer Res.* **2004**, *64*, 7668.
(4) Torchilin, V. P.; Lukyanov, A. N.; Gao, Z. G.; Papahadjopoulos-Sternberg, B. *Proc. Natl. Acad. Sci. U.S.A.* **2003**, *100*, 6039.
(5) Adams, G. P.; Schier, R.; McCall, A. M.; Simmons, H. H.; Horak, E. M.; Alpaugh, R. K.; Marks, J. D.; Weiner, L. M. *Cancer Res.* **2001**, *61*, 4750.
(6) Hirsch, F. R.; Varella-Garcia, M.; Cappuzzo, F. *Oncogene* **2009**, *28* (Suppl1), S32.
(7) Li, S.; Huang, S.; Peng, S. B. *Int. J. Oncol.* **2005**, *27*, 1329.
(8) Muss, H. B.; Thor, A. D.; Berry, D. A.; Kute, T.; Liu, E. T.; Koerner, F.; Cirrincione, C. T.; Budman, D. R.; Wood, W. C.; Barcos, M.; Henderson, I. C. *N. Engl. J. Med.* **1994**, *330*, 1260.
(9) Parker, N.; Turk, M. J.; Westrick, E.; Lewis, J. D.; Low, P. S.; Leamon, C. P. *Anal. Biochem.* **2005**, *338*, 284.
(10) McDaniel, J. R.; Bhattacharyya, J.; Vargo, K. B.; Hassouneh, W.; Hammer, D. A.; Chilkoti, A. *Angew. Chem., Int. Ed.* **2013**, *52*, 1683.
(11) McDaniel, J. R.; MacEwan, S. R.; Dewhirst, M.; Chilkoti, A. *J. Controlled Release* **2012**, *159*, 362.
(12) MacKay, J. A.; Chen, M. N.; McDaniel, J. R.; Liu, W. G.; Simnick, A. J.; Chilkoti, A. *Nat. Mater.* **2009**, *8*, 993.
(13) Falk, M. H.; Issels, R. D. *Int. J. Hyperthermia* **2001**, *17*, 1.
(14) Viglianti, B. L.; Stauffer, P.; Repasky, E.; Jones, E.; Vujaskovic, Z.; Dewhirst, M. *Hyperthermia*; People's Medical Publishing House: Shelton, 2010; Vol. *8*.
(15) McDaniel, J. R.; Radford, D. C.; Chilkoti, A. *Biomacromolecules* **2013**, *14*, 2866.
(16) Meyer, D. E.; Chilkoti, A. *Biomacromolecules* **2004**, *5*, 846.
(17) Meyer, D. E.; Kong, G. A.; Dewhirst, M. W.; Zalutsky, M. R.; Chilkoti, A. *Cancer Res.* **2001**, *61*, 1548.
(18) Fox, M. E.; Szoka, F. C.; Frechet, J. M. J. *Acc. Chem. Res.* **2009**, *42*, 1141.
(19) Ruggiero, A.; Villa, C. H.; Bander, E.; Rey, D. A.; Bergkvist, M.; Batt, C. A.; Manova-Todorova, K.; Deen, W. M.; Scheinberg, D. A.; McDevitt, M. R. *Proc. Natl. Acad. Sci. U.S.A.* **2010**, *107*, 12369.
(20) Lu, J. M.; Peterson, C. M.; Guo-Shiah, J.; Gu, Z. W.; Peterson, C. A.; Straight, R. C.; Kopecek, J. *Int. J. Oncol.* **1999**, *15*, 5.
(21) Mahmud, A.; Xiong, X. B.; Lavasanifar, A. *Eur. J. Pharm. Biopharm.* **2008**, *69*, 923.
(22) To, H.; Ohdo, S.; Shin, M.; Uchimaru, H.; Yukawa, E.; Higuchi, S.; Fujimura, A.; Kobayashi, E. *J. Pharm. Pharmacol.* **2003**, *55*, 803.
(23) Janib, S. M.; Liu, S.; Park, R.; Pastuszka, M. K.; Shi, P.; Moses, A. S.; Orosco, M. M.; Lin, Y. A.; Cui, H.; Conti, P. S.; Li, Z.; MacKay, J. A. *Integr. Biol.-U.K.* **2013**, *5*, 183.
(24) Stone, E.; Chantranupong, L.; Gonzalez, C.; O'Neal, J.; Rani, M.; VanDenBerg, C.; Georgiou, G. *J. Controlled Release* **2012**, *158*, 171.
(25) Dreher, M. R.; Liu, W. G.; Michelich, C. R.; Dewhirst, M. W.; Chilkoti, A. *Cancer Res.* **2007**, *67*, 4418.